Acta Biomaterialia xxx (xxxx) xxx

Contents lists available at ScienceDirect

Acta Biomaterialia

journal homepage: www.elsevier.com/locate/actbio

Full length article

Microtensile properties and failure mechanisms of cortical bone at the lamellar level☆

Daniele Casari[a,*], Johann Michler[a], Philippe Zysset[b], Jakob Schwiedrzik[a,*]

[a] Empa, Swiss Federal Laboratories for Materials Science and Technology, Laboratory for Mechanics of Materials and Nanostructures, Feuerwerkerstrasse 39, CH-3602 Thun, Switzerland
[b] ARTORG Centre for Biomedical Engineering Research, University of Bern, Freiburgstrasse 3, CH-3010 Bern, Switzerland

ARTICLE INFO

Article history:
Received 10 January 2020
Revised 9 April 2020
Accepted 16 April 2020
Available online xxx

Keywords:
Bone
Microtensile strength
Lamellar level
Failure mechanisms
Composite modeling

ABSTRACT

Bone features a remarkable combination of toughness and strength which originates from its complex hierarchical structure and motivates its investigation on multiple length scales. Here, *in situ* microtensile experiments were performed on dry ovine osteonal bone for the first time at the length scale of a single lamella. The micromechanical response was brittle and revealed larger ultimate tensile strength compared to the macroscale (factor of 2.3). Ultimate tensile strength for axial and transverse specimens was 0.35 ± 0.05 GPa and 0.13 ± 0.02 GPa, respectively. A significantly greater strength anisotropy relative to compression was observed (axial to transverse strength ratio of 2.7:1 for tension, 1.3:1 for compression). Fracture surface and transmission electron microscopic analysis suggested that this may be rationalized by a change in failure mode from fibril-matrix interfacial shearing for axial specimens to fibril-matrix debonding in the transverse direction. An improved version of the classic Hashin's composite failure model was applied to describe lamellar bone strength as a function of fibril orientation. Together with our experimental observations, the model suggests that cortical bone strength at the lamellar level is remarkably tolerant to variations of fibrils orientation of about ±30°. This study highlights the importance of investigating bone's hierarchical organization at several length scales for gaining a deeper understanding of its macroscopic fracture behavior.

Statement of Significance

Understanding bone deformation and failure behavior at different length scales of its hierarchical structure is fundamental for the improvement of bone fracture prevention, as well as for the development of multifunctional bio-inspired materials combining toughness and strength. The experiments reported in this study shed light on the microtensile properties of dry primary osteonal bone and establish a baseline from which to start further investigations in more physiological conditions. Microtensile specimens were stronger than their macroscopic counterparts by a factor of 2.3. Lamellar bone strength seems remarkably tolerant to variations of the sub-lamellar fibril orientation with respect to the loading direction (±30°). This study underlines the importance of studying bone on all length scales for improving our understanding of bone's macroscopic mechanical response.

© 2020 Acta Materialia Inc. Published by Elsevier Ltd.
This is an open access article under the CC BY license. (http://creativecommons.org/licenses/by/4.0/)

1. Introduction

Bone is a hierarchically structured connective tissue with remarkable mechanical properties. Its primary functions are structural support, locomotion, organ protection, mineral storage and

Abbreviations: MCF, mineralized collagen fibril; EFM, extrafibrillar matrix; ECM, extracellular matrix; FIB, focused ion beam; SEM, scanning electron microscope; STEM, scanning transmission electron microscopy; HR-SEM, high-resolution SEM; BF-STEM, bright-field STEM.

☆ Part of the Special Issue on Biomineralization: From Cells to Biomaterials, associated with the BIOMIN XV: 15th International Symposium on Biomineralization, held at the Ludwig Maximilian University, Sept 9-13, 2019, organized by Wolfgang Schmahl and Erika Griesshaber.

* Corresponding authors. Empa Swiss Federal Laboratory for Material Science and Technology, Laboratory of Mechanics of Materials and Nanostructures, Feuerwerkerstrasse 39, 3602 Thun, Switzerland. Phone: Tel: +41 58 765 62 31; Fax: +41 58 765 69 90.

E-mail addresses: daniele.casari@empa.ch (D. Casari), jakob.schwiedrzik@empa.ch (J. Schwiedrzik).

https://doi.org/10.1016/j.actbio.2020.04.030
1742-7061/© 2020 Acta Materialia Inc. Published by Elsevier Ltd. This is an open access article under the CC BY license. (http://creativecommons.org/licenses/by/4.0/)

Please cite this article as: D. Casari, J. Michler and P. Zysset et al., Microtensile properties and failure mechanisms of cortical bone at the lamellar level, Acta Biomaterialia, https://doi.org/10.1016/j.actbio.2020.04.030

source: https://doi.org/10.7892/boris.146590 | downloaded: 27.12.2020

blood cell production [1]. Formed and continuously remodeled by a cell-mediated process, bone can self-repair and adapt according to physiological loads throughout life [2,3]. On the macroscale, it consists of a dense and hard cortex incorporating a trabecular (spongy) structure. Cortical bone accounts for approximately 80% of the skeletal mass [1] and has a prominent role in defining the overall tissue mechanical properties [4]. In humans, it is largely composed of osteons, cylindrical structures made of concentric lamellae encompassing central blood vessels (Haversian canals). Individual lamellae are 3-7 µm thick and are composed of bundles of parallel mineralized collagen fibrils (MCFs), typically arranged in plywood-like motifs [5–8]. Embedded into an extrafibrillar matrix (EFM) of non-collagenous proteins, extrafibrillar minerals and water, MCFs make up the nanostructural building blocks of bone extracellular matrix (ECM) [9–11].

By effectively mixing simple components, such as a stiff mineral phase of carbonated hydroxyapatite with a softer organic phase, principally composed of type I collagen and a small amount of non-collagenous proteins, nature constructs a strong and tough nanocomposite [12,13]. Brittle mineral platelets of nanometer dimensions can sustain large stress due to their small size [14] and increase the ECM stiffness significantly [15]. On the other hand, the softer organic phase provides flexibility and allows energy dissipation throughout several toughening mechanisms [16–23]. Through its complex hierarchical organization spanning several length scales, bone is able to increase its toughness by a several-fold increase [20]. As a result, bone is tolerant to defects giving rise to stress concentrations, such as lacunae and canaliculi (containing bone cells and their processes), cavities encompassing blood cells, as well as internal microcracks. Bone's resistance to fracture originates from the great number of interfaces distributed over the whole hierarchical architecture [19,24,25]. Interfaces play a key role in dissipating energy by creating a multitude of deformation and toughening mechanisms that act simultaneously at different length scales [20,26]. Learning how nature attains this attractive combination of mechanical properties from a limited selection of constituents can provide useful insights for the development of multifunctional bio-inspired materials [27,28]. At the same time, a better understanding of bone failure mechanisms and mechanics can lead to improvements in bone fracture prevention in age-related diseases [29,30]. Because of bone's structural complexity, understanding and separating the role of single components, their organization and their interaction across length scales is challenging and requires studies on several different length scales [11].

Recent advances in experimental techniques, such as micropillar compression to measure the uniaxial mechanical response of a material at the micrometer scale [31], allowed to shed light on bone yield and failure properties, as well as on its deformation mechanisms at the lamellar level [32–36]. These studies highlighted a greater strength compared to macroscale that was attributed to a scale-dependent flaw distribution [34]. Micropillar compression also revealed apparent ductility with the absence of damage up to failure [32]. This is in contrast to the quasi-brittle response seen at the macroscale, in which failure is typically caused by growth and coalescence of microcracks generated at interfaces, or in the vicinity of pores [37]. MCFs bridging and kinking, crack deflection and ligament bridging were identified as main toughening mechanisms in compression [32,35]. These experiments have been extremely helpful to better understand bone hierarchical structure but were so far limited to compressive loading. Macroscopically, bone exhibits a loading mode asymmetry and fails at considerably lower stresses under tension. The nanocomposite nature of lamellar bone suggests that a strength asymmetry might also be present at the microscale. Since fracture is typically initiated in tension, characterizing bone under this loading mode is particularly important for clinical studies. To investigate this, we developed a microtensile setup [38] and performed uniaxial tensile experiments on single bone lamellae prepared by focused ion beam (FIB) milling (Fig. 1).

The aim of this study was (a) to characterize the anisotropic tensile yield and failure properties of bone at the length scale of a single lamella, (b) to reveal the respective deformation and failure mechanisms under uniaxial tensile loading, and (c) to postulate a failure model able to predict the anisotropic compression-tension strength asymmetry of the ECM. Microscopic ovine bone tensile specimens were fabricated via focused ion beam milling on primary osteonal bone along axial and transverse orientations. The specimens were successively tested in uniaxial tension inside a scanning electron microscope (SEM). Analytical techniques such as scanning transmission electron microscopy (STEM) and fracture surface analysis by high-resolution SEM (HR-SEM) were employed to reveal nanoscale deformation and failure mechanisms under tension. The findings were compared to previous microscale compression data obtained in similar conditions. Finally, a composite failure model based on physical considerations was identified to capture the micromechanical strength of lamellar bone as a function of fibril orientation for both tension and compression.

2. Materials & Methods

2.1. Sample preparation

An ovine tibia (2 years old) was obtained from a local abattoir and cut at the diaphysis into axial and transverse samples using a diamond-coated band saw (Exact, Germany). Samples were glued onto SEM stubs using cyanoacrylate glue (Ergo 5011, Switzerland) and air-dried. Smooth and flat surfaces were obtained by ultramilling (Polycut E, Reichert-Jung, Germany). A 10 nm thick Au film was sputtered (Leica ACE600, Germany) on the samples to reduce charging during electron and ion beam irradiation. Microtensile specimens of gauge dimensions of 1.5 µm x 5 µm x 10 µm were fabricated at the edges of the samples via top-down FIB milling on ovine primary osteonal bone in axial and transverse orientations, following a previously established protocol [38]. A xenon (Xe) plasma-FIB (Tescan Fera, Czech Republic) operated at 30 kV was employed for the rough milling, while a gallium (Ga) FIB (Tescan Lyra, Czech Republic) operated at 30 kV and successively at 5 kV was used for the final preparation steps to minimize FIB damage. Prior to FIB milling, a platinum (Pt) cap of 1 µm thickness was deposited on the top of the area of interest, to reduce surface roughness ("curtaining") and FIB damage. Sample cutting and fabrication, including specimen orientation, are illustrated in Supplementary Fig. S1. A total of 27 tensile specimens were fabricated (13 axial, 14 transverse). Five specimens (3 axial and 2 transverse) were discarded from the study as they included osteocyte lacunae or visible microcracks.

2.2. Microtensile testing

An *in situ* micromechanical testing platform (Alemnis AG, Switzerland), equipped with a self-aligning single crystal silicon (Si) gripper (Supplementary Fig. S2a, b) [38], was used to pull the specimens in displacement control. Experiments were performed in vacuum, inside an SEM (Zeiss DSM962, Germany) operating at 5 kV to allow for precise positioning and tracking of the deformation mechanisms. Tensile tests were conducted at a quasi-static strain rate of ~ $3{\cdot}10^{-4}$ s^{-1}, which is in the same order of magnitude as the strain rate applied in previous micropillar compression tests on ovine lamellar bone [32]. For each orientation (axial and transverse), five specimens were loaded until failure after being subjected to three partial loading-unloading cycles during a

Please cite this article as: D. Casari, J. Michler and P. Zysset et al., Microtensile properties and failure mechanisms of cortical bone at the lamellar level, Acta Biomaterialia, https://doi.org/10.1016/j.actbio.2020.04.030

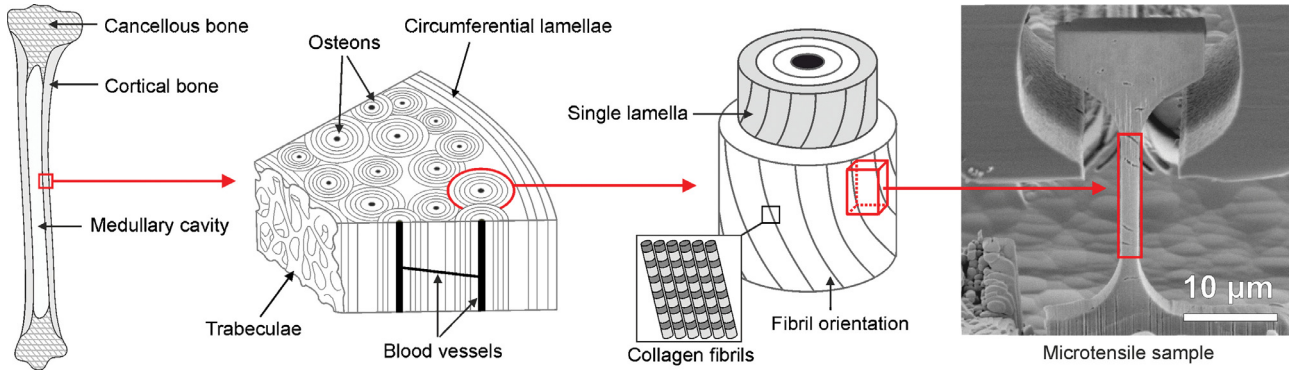

Fig. 1. Hierarchical organization of bone with respect to the microtensile specimen geometry. Bone exhibits a hierarchical structure spanning from the organ level to the molecular level. MCFs and EFM constitute the fibers and matrix of the bone ECM composite. To characterize the tensile properties of bone at the lamellar scale, microtensile specimens featuring gauge dimensions in the order of a few microns are tested under uniaxial conditions.

portion of the linear elastic response. This was performed to measure the elastic modulus since during the unloading segments it is assumed that the specimen deforms elastically. The rest of the specimens were loaded monotonically until failure. Supplementary Video 1 shows an example of a cyclic test (video speed: 30x experimental speed). Force and displacement were monitored at 20 Hz sampling rate. Gauge displacement was computed by correcting the total displacement by the instrument and substrate compliance, as explained in detail elsewhere [38]. Engineering stress was obtained by dividing the measured force by the specimen gauge cross-sectional area, while engineering strain was calculated by dividing the corrected gauge displacement by the initial gauge length. Stress-strain curves were offset to correct for the adaptation response (toe region) observed during initial contact and self-alignment. The corrected zero points of strain were calculated as the intercept of the linear regression of the elastic part of the stress-strain curves with the zero-stress axis [39]. Both engineering values were converted to true stress-strain data using the assumption of negligible volume change.

2.3. Imaging and microstructural characterization

Microtensile specimens were imaged before and after the mechanical tests using a high-resolution SEM (Hitachi S-4800, Japan) operated at 1.5 kV and 10 μA to measure their dimensions and accurately identify the fracture surfaces' main characteristics. Two axial and three transverse specimens with representative failure stresses were chosen for further analysis. Specifically, a TEM lift-out technique was employed to prepare thin sections for STEM analysis [35] in two main orientations (as specified in Supplementary Fig. S2e). Lateral sections were obtained by thinning the fractured gauge section of the specimens, while frontal sections were milled in the base of the specimens. BF-STEM images of the thin sections were taken in a high-resolution SEM (Hitachi S-4800, Japan) using a transmission electron detector while operating the microscope at an acceleration voltage of 30 kV and beam current of 10 μA. Fibril orientation was characterized using the software ImageJ (NIH, Bethesda, Maryland, USA). The plug-in OrientationJ (Biomedical Imaging Group, EPFL, Switzerland), based on structure tensors, was used to evaluate local fibril orientation [40]. A vector field analysis was performed over a selected region of interest of 6×3 μm^2 from the BF-STEM images. A finite difference gradient with a Gaussian window of 125 nm size was applied over a grid of 125 nm periodicity to generate local orientations properties (Supplementary Fig. S3). From this dataset, mean fibril orientation and standard deviation were evaluated using MATLAB (The MathWorks, USA) assuming a normal distribution.

2.4. Failure composite modeling

Strength as a function of MCF orientation was modeled using the improved Hashin's failure criteria [41] developed by Gu and Chen [42]. For a unidirectional fiber-reinforced composite, the plane stress failure criteria can be summarized with the following equations:

Tensile fiber mode $\sigma_{11} > 0$

$$\frac{\sigma_{11}}{T_{11}} = 1 \tag{1}$$

Compressive fiber mode $\sigma_{11} < 0$

$$-\frac{\sigma_{11}}{C_{11}} = 1 \tag{2}$$

Tensile matrix mode $\sigma_{22} > 0$

$$-\frac{2P_t}{S_{21}}\sigma_{22} + \frac{1+\frac{2P_tT_{22}}{S_{21}}}{T_{22}^2}{\sigma_{22}}^2 + \frac{\tau_{21}^2}{S_{21}^2} = 1 \tag{3}$$

Where P_t can be described by

$$P_t = \left(\frac{1}{C_{22}} - \frac{C_{22}}{4S_{23}^2}\right)\frac{S_{21}}{2} \tag{4}$$

Compressive matrix mode $\sigma_{22} < 0$

$$\left(-\frac{1}{C_{22}} + \frac{C_{22}}{4S_{23}^2}\right)\sigma_{22} + \frac{\sigma_{22}^2}{4S_{23}^2} + \frac{\tau_{21}^2}{S_{21}^2} = 1 \tag{5}$$

Where σ_{11}, σ_{22} and τ_{21} denote the resolved normal and shear stresses. T_{11} and C_{11} stand for the uniaxial tensile and compressive strengths along the longitudinal fiber axis. Whereas, tensile and compressive strengths in the transverse orientation are indicated by T_{22} and C_{22}, respectively. Finally, S_{21} and S_{23} represent the shear strengths oriented parallel and perpendicular to the fibril direction, respectively (illustrated in Supplementary Fig. S4).

To evaluate the model, compressive strength C_{11} and C_{22} were set to 0.49 GPa and 0.30 GPa, respectively. These values correspond to the compressive yield stresses measured by Schwiedrzik et al. [32] via micropillar compression. The shear strength between the fibril and the extrafibrillar matrix along the fibril direction (S_{21}) in dry conditions was calculated based on the existing literature. The influence of hydration on compressive strength was observed by Schwiedrzik et al. [35], in which $\sigma_{\text{hydrated}}/\sigma_{\text{dry}} = 0.4$. If this ratio is combined with the shear stress measured by Gupta and al. [18] in the hydrated state (80 MPa), it is possible to predict S_{21} in dry conditions (200 MPa). The shear strength perpendicular to the fibril direction S_{23} was set to 280 MPa based on the critical shear strength found for transverse micropillar compression in dry conditions [32]. At first, the failure criteria were evaluated in Mathe-

Please cite this article as: D. Casari, J. Michler and P. Zysset et al., Microtensile properties and failure mechanisms of cortical bone at the lamellar level, Acta Biomaterialia, https://doi.org/10.1016/j.actbio.2020.04.030

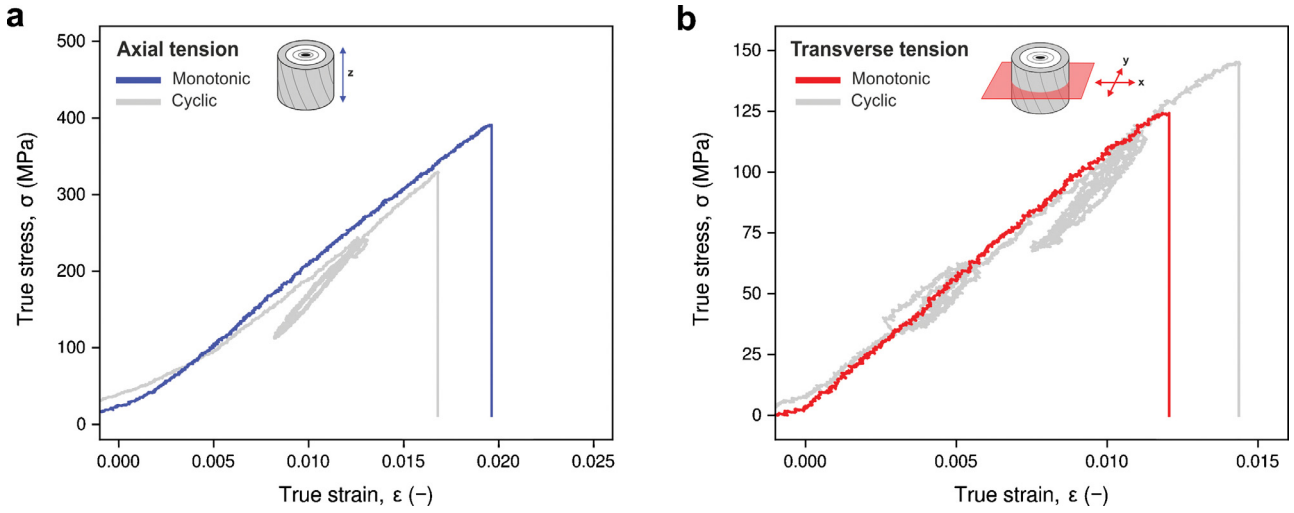

Fig. 2. Microtensile anisotropic response of lamellar bone. Representative true stress-strain curves for axial (a) and transverse (b) tension of ovine bone at the length scale of a single lamella.

matica (Wolfram Research, Inc., Version 12.0, Champaign, IL) by using the average measured micromechanical data and their assumed fibril orientation based on sample type (axial = 0°; transverse 90°). The model was later optimized via least square optimization by fitting specific strengths and respective average MCFs orientation of three microtensile specimens for which the microstructure was investigated by STEM. For the first case, all parameters were predetermined. For the second case, T_{11} and T_{22} were fitted, while the rest of the parameters were set.

2.5. Statistics

All data manipulations and statistical analysis were performed using MATLAB. Normality of the distributions was tested by the Kolmogorov-Smirnov normality test. Measurements are reported as mean ± standard deviation. Significant differences between datasets were tested using two-tailed t-tests. The significance threshold was chosen with an error probability $p \leq 0.05$.

3. Results and Discussion

3.1. Microtensile properties of lamellar bone

Uniaxial tensile tests were performed at quasi-static strain rates of $3 \cdot 10^{-4}$ s^{-1} on specimens having thicknesses of 5.29 ± 0.42 µm (mean ± standard deviation), widths of 1.80 ± 0.13 µm and gauge section lengths of 10.02 ± 0.25 µm. All tested specimens failed within the gauge section. Representative true stress-strain curves obtained from both monotonic and cyclic tests are displayed in Fig. 2. The full collection of the stress-strain curves can be found in Supplementary Figure S5. It can be observed that specimens exhibited apparent brittle failure. Microtensile tests showed anisotropy in both strength and stiffness. Axial specimens were significantly stiffer ($p = 1.15 \cdot 10^{-5}$) and stronger ($p = 8.46 \cdot 10^{-11}$) when compared to their transverse counterparts. Elastic modulus was 27.7 ± 3.4 GPa in axial orientation and 13.6 ± 1.1 GPa in transverse orientation. Strength was 0.35 ± 0.05 GPa at 1.8 ± 0.2% strain for axial specimens, and 0.13 ± 0.02 GPa at 1.3 ± 0.3% strain for transverse specimens. As expected, both stiffness and strength showed a prominent anisotropy.

The apparent elastic moduli measured in this study were similar to the ones reported by micropillar compression performed on ovine bone [32] and bovine bone [33] in the same testing conditions. Several studies can be found in the literature using nanoindentation as a way to characterize both elastic modulus and hardness for osteonal bone in dry conditions [43–49]. One should however compare the elastic moduli obtained via nanoindentation with the data in this study with some caution for the following reasons. Most of the studies focused on human Haversian bone. While ovine and human bones show comparable mineral to matrix ratios (Supplementary Information A: Raman spectroscopy), Haversian bone in humans exhibits more complex MCF orientation patterns (plywood like organization), whereas primary lamellar ovine bone has a rather uniaxial MCF orientation [35]. The cited nanoindentation studies are based on the Oliver-Pharr method [50] and often assume the tested material tested to be isotropic. The complex stress state below the indentation surface, especially in the case of heterogeneous and anisotropic material such as bone, involves non-uniform deformations in all principal axes. This explains why in most studies, the reported elastic modulus along axial (longitudinal) orientation was lower than the one reported here. The opposite trend was observed for the elastic modulus reported for transverse orientation. However, when interpreting the nanoindentation results using an anisotropic stiffness tensor [51], the literature data fit well to what was found in this study [32,51]. The measurements reported in Table 1 also fit well with the model proposed by Reisinger et al. [52,53] for a uniaxial mineralized fibril-array in dry conditions, as well as with the model by Hamed et al. [54] for aligned fibrils with a correction of a 20% increase in stiffness in all directions for dry condition [44].

The measured strength on the microscale was considerably larger than what has been reported at the macroscale [55]. A greater strength at lower length scales highlights the influence of the hierarchical organization of bone and is associated with a scale effect. In bone, the absence of microdamage, cement lines, and large pores [56], such as Haversian canals and osteocyte lacunae, results in a factor of 2.3 higher strength of microscale specimens. A similar scaling ratio has been reported for compression experiments [32]. Although the volume tested here was smaller (38%) than the one tested in compression, we believe that a direct comparison between the tensile experiments performed in this study and earlier measurements in compression is justified. Even by assuming MCF diameters up to 200 nm and a fiber volume ratio of no more than 50%, at least 100 structural units (MCFs) are present in the tested volume. It would be surprising to observe a specimen size effect for this scale. The number of MCFs is also comparable with the number of osteons, structural units at a higher length scale, found in i.e. a standard macroscopic sample measuring 3 mm

Please cite this article as: D. Casari, J. Michler and P. Zysset et al., Microtensile properties and failure mechanisms of cortical bone at the lamellar level, Acta Biomaterialia, https://doi.org/10.1016/j.actbio.2020.04.030

Table 1
Micromechanical properties of cortical bone on the microscale. Compression and tensile properties of primary lamellar bone tested in vacuo; mean ± standard deviation of elastic modulus E, maximum stress σ^{max}, strain at maximum stress ε (σ^{max}) and yield stress σ^{y}. Whereas, N is the number of specimens tested in the respective loading mode. These data were collected at quasi-static strain rates of ≈ 3-5 · 10^{-4} s^{-1} in both axial and transverse orientations via in situ microtensile tests and micropillar compression.

Sample Orientation	Loading mode	E (GPa)	σ^{max} (GPa)	ε (σ^{max}) (%)	σ^{y} (GPa)	N (-)
Axial	Compression*	31.1 ± 6.5	0.75 ± 0.06	5.4 ± 1.7	0.49 ± 0.10	19
	Tension	28.9 ± 3.4	0.35 ± 0.05	1.8 ± 0.2	-	10
Transverse	Compression*	16.5 ± 1.5	0.59 ± 0.04	12.1 ± 2.5	0.30 ± 0.02	20
	Tension	13.6 ± 1.2	0.13 ± 0.02	1.3 ± 0.3	-	12

* Data from Schwiedrzik et al. [32].

in diameter [32]. In fact, osteons diameter ranges between 170 um and 270 µm, whereas their density typically varies between 15 to 25 units per mm^2 depending on age [57–60]. Our hypothesis is further supported by the reported absence of a strength size effect in the range between 1 and 5 µm diameter reported for compression of bone micropillars [34].

3.2. Tension-compression asymmetry

Bone, like other brittle materials, is stronger in compression than in tension. Comparing the microtensile data with previous micropillar compression experiments, it can be observed that the tension-compression strength asymmetry is also seen at the microscale and is therefore an inherent tissue property. This is well shown in Table 1, where the micromechanical properties of ovine bone are summarized for both tension and compression experiments for dry testing. At the lamellar scale, bone is strongest when compressed along its main axis, exhibiting strength of 0.75 ± 0.06 GPa. Contrarily, it performs poorly when it is tested in tension normal to the main MCF orientation and fails at 0.13 ± 0.02 GPa. From Table 1 it can be observed that the loading mode had minimal influence on the elastic response of bone. The elastic modulus for the axial orientation showed no statistical difference ($p = 0.50$) between compression and tension. Transverse elastic modulus showed a significant ($p = 9.2 \cdot 10^{-3}$) but relatively small difference between the two loading modes. This is most likely due to the limited amount of samples tested in tension compared to compression.

When the post-yield behavior at the length scale of single lamellae is compared between loading modes, there is a significant difference between tension and compression. For compression, a significant ductility was found. This is not the case for tensile loading for which apparent brittle failure is observed. Interestingly, strength anisotropy was much more pronounced in tension. In compression, the ratio between ultimate axial and transverse strength is 1.3, whereas, in tension, this value increases to 2.7. A factor of 2.1 is thus seen between the two loading modes. A similar trend is also noticed when ultimate strength is replaced by yield stress (factor of 2.9). The increased strength anisotropy seen in tension compared to compression hints at a change in failure mechanism calling upon a more in-depth analysis.

3.3. Failure mode anisotropy

Images of the fracture surfaces, obtained by high-resolution SEM, confirm that axial and transverse specimens failed in two different ways. Fig. 3 shows the fracture surfaces for three axial specimens (Fig. 3a,b,c) and three transverse specimens (Fig. 3d,e,f). Here, different morphologies can be distinguished based on the sample orientation. Axial surfaces appear rough and reveal an overall porous structure. Pore size ranges between 40 to 60 nm and is comparable to the diameter of individual MCFs [61]. As in primary ovine bone MCFs appear mainly oriented along the longitudinal

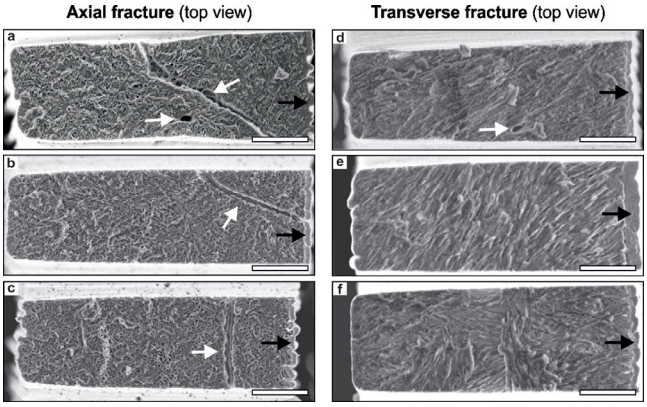

Fig. 3. Fracture surfaces of axial and transverse specimens. SEM Top view of the fracture surfaces for axial samples (a,b,c) in which canaliculi are seen (white arrows). Contrarily, in transverse samples (d, e, f) the lacuno-canalicular network is seen only occasionally. In all specimens, a thin FIB redeposition layer (50-200 nm thickness) is seen in the back of the specimen (black arrows). Scale bars represent 1 µm.

axis of osteons [35], the observed surface topography (Fig. 3a,b,c) can be rationalized with a fibril-matrix shear interface failure. In this case, interfaces failure between MCF and EFM leads to successive MCFs being pulled out, resulting in a rough and porous fracture surface. In axial specimens, canaliculi were present on each fracture surface. In the transverse orientation, a different scenario is observed. Transverse specimens exhibit globally smoother fracture surfaces with fewer steps and show a rich fiber texture in the fracture plane. Furthermore, canaliculi were present in only 42% of the fracture surfaces. In all transverse specimens, the fracture plane was found to be highly orthogonal to the loading direction (<3°). As MCFs are mostly aligned perpendicular to the loading orientation it is very likely that the surfaces displayed in Fig. 3d,e,f are the product of a fibril–matrix interfacial decohesion in tension, in contrast to interfacial shear failure in the axial direction. Microtensile specimens reveal therefore a failure mode change when loaded in different orientations. In compression such a change is absent, and matrix shear failure is always observed [32]. The higher strength anisotropy dependency observed in tension compared to compression might be explained by this divergence.

3.4. Influence of canaliculi and weak interfaces

In axial specimens, cracks are always initiated at canaliculi. Since canaliculi are typically oriented radially inside osteons [62], they mainly lie perpendicular to the loading direction in axial samples. These microstructural features lead to large stress concentrations in the material, but they serve a biological function by accommodating osteocytes processes. In the transverse orientation, canaliculi were seen in only 42% of the fracture surfaces. Inter-

Please cite this article as: D. Casari, J. Michler and P. Zysset et al., Microtensile properties and failure mechanisms of cortical bone at the lamellar level, Acta Biomaterialia, https://doi.org/10.1016/j.actbio.2020.04.030

estingly, when a canaliculi was present on the fracture surface the measured strength ($\sigma^{max} = 0.11 \pm 0.01$ GPa) was significantly lower ($p = 1.92 \cdot 10^{-3}$) than in the rest of the cases ($\sigma^{max} = 0.15 \pm 0.02$ GPa). No significant difference was found in terms of stiffness ($p = 0.81$). The difference in strength between these typologies of transverse specimens might be explained by the fact that the transverse specimens' orientation ranges between circumferential and radial directions. While MCF arrangement is expected to be transversely isotropic, porosity is not. In circumferential specimens, canaliculi are present almost perpendicular to the loading direction. Similarly to axial specimens, the high stress concentrations in the vicinity of the canaliculi dominate failure and create a fracture surface containing a canaliculus. Contrarily, in radial specimens, the canaliculi predominantly run along the loading direction and failure seems to be dominated by other effects. Bright-field STEM (BF-STEM) performed on both tested and non-tested sections of material (Supplementary Fig. S6) revealed no observable differences in the MCF organization, suggesting the absence of significant ductile deformation before failure occurred. Interestingly, regions with ordered and disordered MCF motifs were observed. This is in line with earlier studies [8,35,63] and shows a key design feature for crack deflection at the microscale. The interface between a disordered and ordered phase acts as a weak layer in the structure that serves to deflect a crack away from the original plane of fracture. This is comparable to the effect of lamellar interfaces [23,64,65] at the same length scale, as well as cement lines [66–68] at higher length scales. From the STEM images, it appears that these weak interfaces are typically oriented with the long axis of osteons. When loaded in tension, as is the case in the radial specimens, these interfaces fail by delamination of MCF and EFM. If this happens, fracture surfaces will reveal a clear fiber texture, as seen in Fig. 3e.

3.5. Microscale fracture toughness

Using the modeling assumption that a canaliculus passing through a specimen acts as a through-crack inside a finite plate [69], it is possible to estimate the magnitude of the conditional fracture toughness K_{IQ} (mode I) for all axial specimens, as well for the transverse specimens exhibiting canaliculi on the fracture surface. Using the solution reported by Tada et al. [70] the mode I stress intensity factor K_I for a crack through a finite plate can be described as:

$$K_I = \sigma\sqrt{\pi a}\left[\sec\left(\frac{\pi a}{2T}\right)^{1/2}\right]\left[1 - 0.025\left(\frac{a}{T}\right)^2 + 0.06\left(\frac{a}{T}\right)^4\right] \quad (6)$$

Where σ is the stress applied, a is the half-width of the crack and T is the half-thickness of the plate, in our case the thickness of the specimen. Considering the canalicular diameter measured on the fracture surfaces (160 ± 59 nm), the critical stress intensity factor is 0.17 ± 0.03 MPa $m^{1/2}$ and 0.07 ± 0.01 MPa $m^{1/2}$ for axial and transverse orientations, respectively. These values likely are only a rough estimate of microscale bone's fracture toughness in dry conditions as they neglect the finite radius of the initial flaw and the misorientation of the canaliculi to the surface normal, and might be calculated for plane stress conditions. However, they serve to highlight a significant scale effect similar to earlier findings [35,71]. The fracture toughness at the microscale estimated here is at least an order of magnitude smaller than the one observed at the macroscale [20,66]. This is likely caused by the absence of extrinsic toughening mechanisms such as crack deflection at cement lines, crack-ligament bridging and constrained microcracking when small volumes of ECM are tested. This result underlines the importance of bone's architecture for its fracture resistance.

3.6. Microstructure and strength composite modeling

In order to relate the mechanical behavior and failure mechanisms to the fundamental microstructure, thin sections of material were prepared from several failed tensile specimens and imaged using BF-STEM. Lateral sections were manufactured by thinning the width of the specimen fractured gauge sections, while frontal sections were fabricated from the underlying substrate (schematics in Supplementary Fig. S2e). Fig. 4 illustrates three BF-STEM images taken from lateral thin sections of two axial specimens (Fig. 4a,b) and a transverse specimen (Fig. 4c). Darker areas are associated with higher average mass due to stronger electron scattering. Because collagen molecules are staggered axially along fibrils [72], it is possible to see the fibrous structure of lamellar bone when MCFs primarily lie in the image plane. Ordered regions are identified through the presence of characteristic gap zones (less dense regions) and their respective periodic banding pattern of 67 nm (alternating dark-bright contrast). In general, STEM observations suggested that, differently from secondary osteons, for which MCFs seem to organize in ply-wood like motifs [5–8], the investigated primary ovine osteons exhibit an overall homogeneous MCF orientation with a general texture along the osteon main axis. In the two axial specimens seen in Fig. 4, MCFs are oriented at two different ($p < 1 \cdot 10^{-15}$) angles of 8.7 ± 6.4° (Fig. 4a) and 24.5 ± 17.9° (Fig. 4b) with respect to the loading direction. Their respective frontal sections also exhibited a difference ($p < 1 \cdot 10^{-15}$) in MCF orientation with angles of 5.6 ± 8.8° and 12.7 ± 10.9°, respectively. In the transverse specimen, fibril orientation was 88.2 ± 11.7° (Fig. 4c). Frontal STEM images can be found in Supplementary Fig. S7.

Interestingly, the specimen shown in Fig. 4a has a more coherently oriented MCF microstructure with an average a smaller offset from the loading direction than the sample displayed in Fig. 4b, but it failed at lower stress (81% of the maximum). This behavior seems counterintuitive at first glance, as one would expect the material to be stronger along the main fibril orientation. However, bone is different from a common engineering composite, which commonly features stiff and strong fibers embedded into a much more compliant matrix. Here the difference in strength between fiber and matrix is less striking. Moreover, the high mineral content present in the EFM allows relatively high shear strength (up to 280 MPa in dry conditions [32]), causing a maximum in strength when the underlying MCF organization is tested at an angle $\theta \neq 0°$.

Because of its sub-lamellar MCF organization, being mostly uniaxial, ovine primary osteonal bone on the microscale might be considered as a unidirectional fiber reinforced composite. The classic failure composite model proposed by Hashin's [41] is a well-established model which considers four distinct failure modes – tensile and compressive fiber and matrix modes – and can be used to describe the strength as a function of MCF orientation in bone. The improved and re-examined version of the Hashin's model, proposed by Gu and Chen [42], was applied to the data collected in this study to describe bone strength as a function of MCF orientation.

At first, the Hashin's model was evaluated using the data in Table 1 and assuming MCF orientation of $\theta = 0°$ and $\theta = 90°$ for axial and transverse specimens, respectively (dashed lines in Supplementary Fig. S8). Despite this generic assumption, the model showed a characteristic trend with maximum strength for MCF main orientation $\theta \neq 0°$. This is true despite the fact the MCF main orientation is slightly different for each specimen. A more accurate description of the tensile behavior of lamellar bone is given in Fig. 5, where the MCF main orientation obtained by STEM is considered for the fit. Instead of using the averaged data from Table 1 to evaluate the model, in Fig. 5 the model is fitted with

Please cite this article as: D. Casari, J. Michler and P. Zysset et al., Microtensile properties and failure mechanisms of cortical bone at the lamellar level, Acta Biomaterialia, https://doi.org/10.1016/j.actbio.2020.04.030

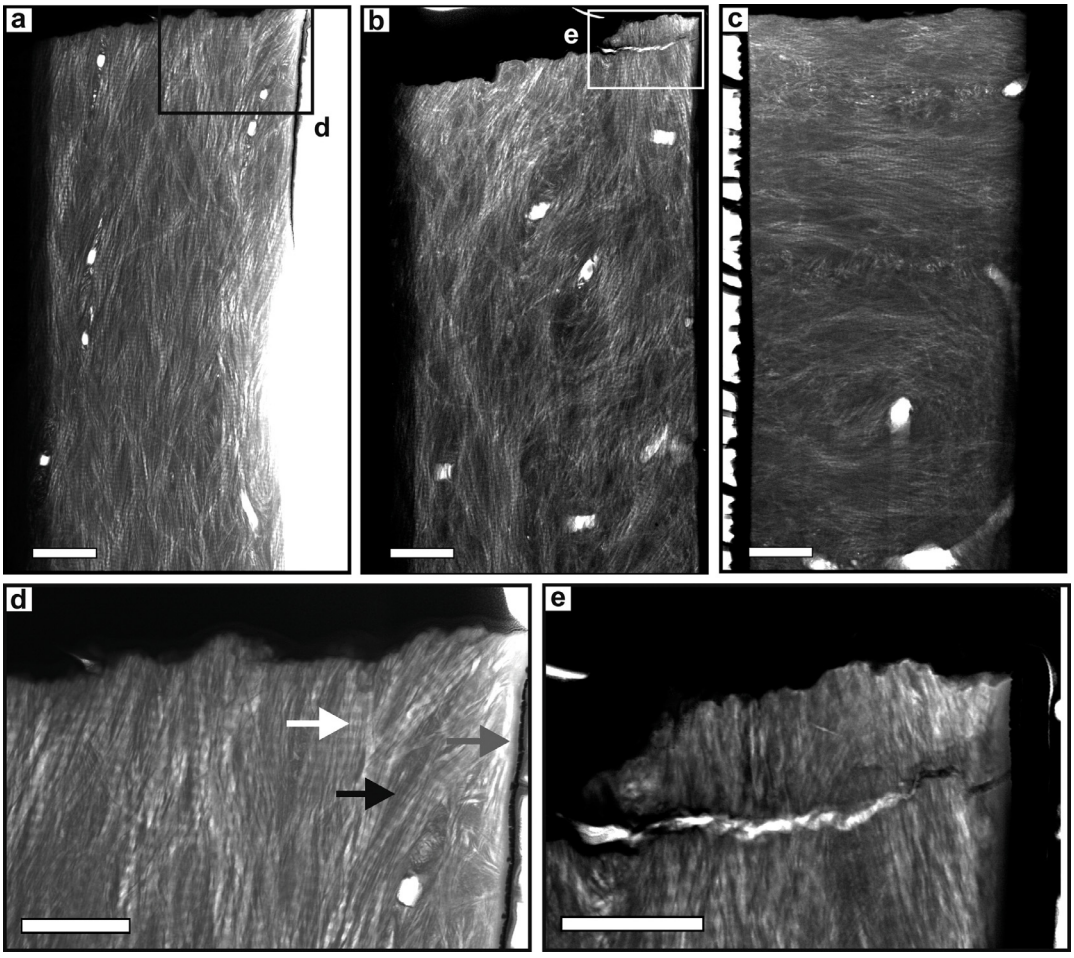

Fig. 4. STEM imaging of deformed microtensile specimens. BF-STEM images of three lateral thin sections for axial (a, b) and transverse (c) specimens after fracture. The in-plane fibrils' organization is visible through the characteristic 67 nm collagen banding pattern. In (a), (b) and (c) scale bars represent 1 μm. A higher magnification image (d) highlights the collagen banding pattern (white arrow) and the presence of mineral crystals (black arrow). Unfortunately, crystal geometry could not be fully resolved because of the limited resolution of low voltage STEM. An amorphous layer accounting for less than 35 nm (produced during FIB milling) and a thin layer of Pt are also visible at the edge of the section (grey arrow). A high magnification image of a crack (e) observed in the axial orientation shows roughness at the level of single fibrils as well as fibril bridging. In (d) and (e) scale bars represent 500 nm.

the individual strengths and respective MFC angles of the three tensile specimens (illustrated in Fig. 4a, b, c), via least-square optimization. This might be a more representative description of the material strength than the one described earlier because STEM can access specific MCF organization through the specimen gauge section. The material properties can, therefore, be related to a specific microstructure rather than an assumed average microstructure. To summarize the dehydrated mechanical properties of lamellar bone, both tension and compression are illustrated in Fig. 5. Strength uncertainties for the displayed individual data points (vertical error bars for the tension case) were calculated by error propagation analysis, with the assumption of random independent errors [73] using force and SEM measurements uncertainties (4μN for force measurement and 100 nm for geometrical deviations).

The optimized model predicts a tensile strength of 330 MPa and 125 MPa for specimens having fibrils aligned parallel and perpendicularly to the load direction, respectively. The maximum tensile strength of 407 MPa is found at an angle of 26°, whereas the maximum compressive yield strength of 553 MPa is found at an angle of 21°. These limits denote the change between fiber failure mode and matrix failure mode. While this result seems striking, a similar behavior was first predicted by Wagner and Weiner [74] and later observed in the case of lamellar stiffness [52,75], with the latter being the largest at an angle between 10° and 30° with respect to the main osteon axis. The general trend illustrated by the model in Fig. 5 also correlates well with the observations of Wagermaier et al. [76], Spiesz et al. [77] for which the average MCF main orientation over several human osteonal lamellae was measured with an offset of 20-30° with respect to the bone's long axis. Similar results were also observed by Turner et al. [78] for canine osteonal bone. Interestingly, the high tolerance (±30°) in fibril orientation with respect to the nanocomposite strength remains well noticeable even when taking into account the weakening effect proposed by Gu and Chen [42] into Hashin's model (Supplementary Fig. S9). Such tolerance might suggest the advantage of rearranging the MCF organization inside a lamella from a uniaxial pattern to a plywood-like pattern [5–8]. More precisely, the variation of fibril angles across the newly formed tissue could be a way to improve bone's fracture toughness, while still retaining the majority of its overall strength [79,80].

The illustrated model is most likely an oversimplified representation of the behavior of lamellar bone but it gives an estimate of the strength of dry bone. The model neglects factors such as variation in mineralization, MCF waviness and distribution along the main orientation. While a model based on continuum micromechanics might be used to account for these additional effects [81,82], the simple model considered here seems well suited to capture the general trend of the anisotropic loading

Please cite this article as: D. Casari, J. Michler and P. Zysset et al., Microtensile properties and failure mechanisms of cortical bone at the lamellar level, Acta Biomaterialia, https://doi.org/10.1016/j.actbio.2020.04.030

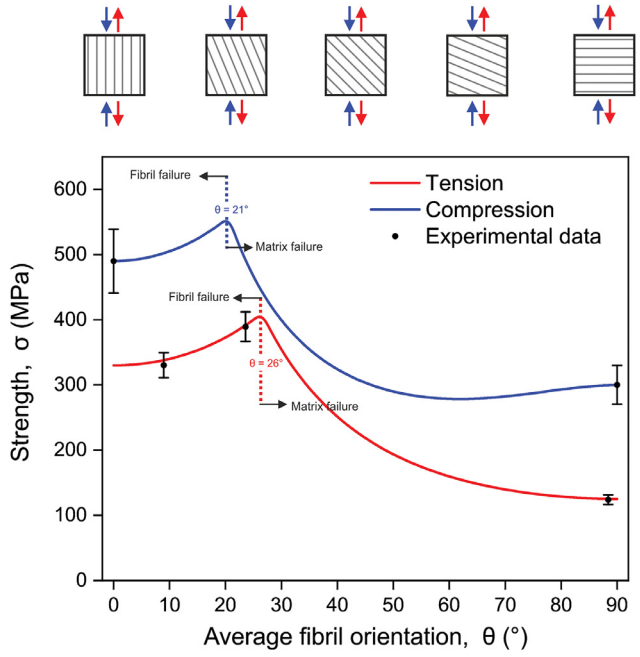

Fig. 5. Composite failure model of ovine lamellar bone on the microscale in tension and compression. Compressive (blue) and tensile (red) strength of lamellar bone as a function of fibril orientation. The graph is illustrated with the schematics of the offset angle θ between loading orientation and MCF main orientation. Individual strengths of the tensile specimens displayed in Fig. 4 are indicated with their respective MCF main orientation. Compressive yield strengths taken from the literature [32] were also fitted with the composite failure model. The error bars in the tension curve denote the experimental uncertainty of individual measurements and are obtained by error propagation analysis.

mode-dependent strength in bone at the microscale. Even when the model was optimized to fit the five data points shown in Fig. 5, it still exhibits the same characteristic trend when biological variations are considered (i.e. fitting the model with the data in Table 1, illustrated in Supplementary Fig. S9). While failure has shown to be dominated by canaliculi due to stress concentrations, the model implicitly takes into account their effect and since these flaws are fairly consistent in size and well distributed in cortical bone for many species, including humans [83,84], the Hashin's composite failure model presented here can be considered to be well representative of the tissue behavior in an average sense.

3.7. Limitations of the study

A well-known limitation in micromechanics is the limited quantity of samples due to the time consuming preparation process. Here, both axial and transverse samples were collected from the same tibia. Nevertheless, since osteons are created individually and only in two cases two specimens were fabricated on the same osteon, the authors believe the specimens may be treated as non-related. Primary ovine osteonal bone was chosen over human osteonal bone for its simpler and rather homogenous MCF organization, thus making the data interpretation more straightforward. Learning about the basic deformation and failure mechanisms in less complex model materials is a prerequisite for improving our understanding of human bone. Based on the behavior of an individual (uniaxially oriented) lamellar ply, we are able to construct the behavior of more complex laminates containing several plies using modeling approaches. If in humans the MCFs are arranged in plywood-like organization inside the osteons, classic laminate theory or more complex finite element models can be used to build a specific model able to predict the behavior of human bone. This is however beyond the scope of this manuscript. In terms of mineral to matrix ratio, human and ovine bone are similar and a direct comparison between the two, for a unidirectional lamellar ply, seems justified. This was confirmed by Raman spectroscopy, which revealed mineral/matrix ratios (v2PO4/Amide III; Supplementary Fig. S10) of 0.63 ± 0.05 and 0.76 ± 0.08 for axial and transverse samples, respectively (Supplementary Information A). These mineral/matrix ratios are in the same range as what is reported in the literature for human osteonal bone [85,86] and human trabecular bone [87].

Another limitation to be considered is that specimens are fabricated via FIB milling. Fabrication artifacts such as redeposition (Fig. 3) and FIB damage (Fig. 4d) might affect the mechanical properties of the specimens. Based on previous Monte Carlo simulations for Ga^+ irradiation on bone [32], as well as from Fig. 3 and 4, it was possible to deduce that these artifacts combined only account for less than 6% of the total gauge cross-section area. Their effect is therefore likely to be negligible.

Under tensile loads, dry lamellar bone exhibited mode I fracture perpendicular to the loading direction and failed catastrophically due to unstable crack growth. While the latter might have been partially encouraged by the system compliance [88], the use of our setup ensured that failure occurred in the gauge section for all specimens even when misalignment might have been present. This provides an accurate value of the material strength in dry conditions.

The major limitation of this study is the fact that both specimen fabrication and mechanical testing has been performed in a vacuum environment. The drying process clearly affects both elastic and yield properties of bone [35,89,90]. Individual collagen fibrils have shown significant shrinking and stiffening with decreasing hydration [91]. Water is an essential element for collagen viscoelasticity [92] which in turn is reflected on bone's mechanical response [93]. In terms of toughness, the presence of water in the extrafibrillar matrix seems to contribute to plasticity in bone [94] by acting as a lubricant between mineral particles, thus promoting inter-fibrillar sliding [95]. In general, hydration increases the nanocomposite toughness through the presence of dissipative mechanisms [18,96,97]. Surface roughness in Fig. 4d,e, hints at the existence of such microscale toughening mechanisms in the form of fibril pull-out and fibril bridging, although these mechanisms are likely inhibited by the drying process. It is expected that under hydrated condition they will influence crack resistance, especially in tension. Seto et al. [89] tested the ECM in tension at the mesoscale under hydrated conditions and observed plastic deformation without premature failure at low strains. Based on previous results, one could make a rough estimate of the properties of bone at the microscale in tension under hydrated condition. In general, it has been observed that hydration decreases Young's modulus, decreases strength, increases bone's toughness and increases strain to fracture [35,44,49,89,90,98,99]. On the microscale, comparative nanoindentation studies between dry and hydrated conditions revealed that wet samples exhibited a decrease in elastic modulus compared to dry conditions between 15% and 30%, as well as a decrease in hardness ranging from 10% to 60%. The large scatter in the reported data is likely associated with the complex organization of the MCFs found in human bone and the heterogeneous stress state below the indented surface. Previous micropillar compression experiments at the lamellar scale in both dry [32,34] and hydrated conditions [35,36] showed that plastic deformation in bone is predominantly dominated by shear in the EFM, or at the MCFs interfaces. This was also observed in mesoscopic tensile tests coupled with X-ray scattering and diffraction analysis [18,100]. If the plastic deformation is predominantly dominated by shear in both compression and tension, it might be possible to make a better prediction of the effect of dehydration on the microtensile specimens tested in this study by using the information

Please cite this article as: D. Casari, J. Michler and P. Zysset et al., Microtensile properties and failure mechanisms of cortical bone at the lamellar level, Acta Biomaterialia, https://doi.org/10.1016/j.actbio.2020.04.030

from micropillar compression rather than the one from nanoindentation. Based on the existing micro compression data on primary ovine bone [35], uniaxial microtensile tests performed under quasi-physiological conditions should lead to a significantly increased ductility, a reduction of the elastic modulus of at least 20% and a strength decrease in the order of 60%, when compared to dry conditions.

Still, in order to investigate bone's microscale properties and deformation mechanisms under physiological conditions, it is crucial to extend the current testing methodologies to the hydrated state. A setup allowing uniaxial tensile testing of lamellar bone in the hydrated condition is currently under development to verify these hypotheses.

4. Conclusions

The tensile properties of ovine lamellar bone were characterized at the length scale of a single lamella under uniaxial loading using a microtensile setup inside an SEM. Microtensile testing was combined with post-test STEM observation to analyze deformation and failure mechanisms, as well as to define a composite failure model able to predict strength and failure mode as a function of the main MCF orientation. *In vacuum* microtensile experiments on ovine lamellar bone revealed brittle failure, a highly anisotropic response and a significant size effect compared to macroscale data (factor of 2.3 higher strength). Axial specimens exhibited strength of 0.35 ± 0.05 GPa, whereas transverse specimens exhibited strength of 0.13 ± 0.02 GPa. Similarly to what was observed at the macroscale, strength anisotropy was considerably greater for tension than for compression. This discrepancy between the two loading modes may be attributed to a change in failure mode from fibril-matrix interfacial shearing for axial specimens to fibril-matrix debonding for transverse specimens. In compression this change is absent, with fibril-matrix interfacial shearing being the failure mode for both axial and transverse specimens. BF-STEM imaging revealed that for the small volumes tested in this study, the sub-lamellar MCF organization of primary lamellar bone is fairly uniaxial and with an orientation close to the longitudinal axis of the bone. Yet, disordered phases were also observed and they seem to have an important influence on the failure mechanisms, especially for transverse specimens. Disordered phases give rise to weak interfaces and might be a key design feature for crack deflection. Their influence is similar to cement lines and lamellar interfaces, in which cracks can be deviated from critical orientations and dissipate deformation energy. Analysis of the failure mechanisms showed also the influence of the lacuno-canalicular system, especially in axial specimens for which failure is always initiated by canaliculi which run in radial direction creating the highest stress concentrations. Using linear elastic fracture mechanics it was possible to estimate the mode I fracture toughness K_I in the case of axial fracture (0.17 ± 0.03 MPa $m^{1/2}$) and transverse fracture (0.07 ± 0.01 MPa $m^{1/2}$). The noticeable reduction of the fracture toughness from the macroscale by at least one order of magnitude might be rationalized by the absence of the major extrinsic toughening mechanisms found at higher length scales, such as uncracked-ligament bridging [101] or crack-deflections/twists at the cement lines [66–68]. Finally, an improved version of the well-established Hashin's composite failure model was applied to describe lamellar bone strength as a function of MCF main orientation. Despite its limitations, due to the simplified representation of the microstructure of lamellar bone as a uniaxial composite, the model shows good agreement with the experimental data. The data suggest that lamellar bone strength on the microscale is remarkably tolerant to variations of fibril orientation of about ±30°. The presented study establishes a baseline for the microtensile properties of bone at the lamellar scale and underlines the importance of bone's hierarchical microstructure and the need to study structure-property relationships on all length scales for gaining a deeper understanding of its macroscopic behavior.

Author Contributions

The initial planning of the study was done by J.S., J.M. and P.Z. Microtensile specimens were fabricated by D.C. and J.S. In situ experiments and SEM/STEM imaging were performed by D.C. Data analysis and interpretation was performed by D.C. in cooperation with J.S. The manuscript was written by D.C. with contributions from all the authors.

Funding Sources

This study was funded by the Swiss National Science Foundation (SNSF) grant no. 165510 and Ambizione grant no. 174192.

Declaration of Competing Interest

The authors declare no competing financial interests.

Acknowledgment

This study was funded by the Swiss National Science Foundation (SNSF) grant no. 165510 and Ambizione grant no. 174192. The authors acknowledge the Scientific Center for Optical and Electron Microscopy (ScopeM) at ETH Zürich for providing access to their facilities. The authors would like to thank Dr. J. Reuteler for his assistance during plasma-FIB milling and STEM lamellae thinning, L. Pethö for making possible the fabrication of microtensile grippers, G. Buerki for his technical assistance during FIB milling and T. Kochetkova for her assistance during Raman spectroscopy.

Supplementary materials

Supplementary material associated with this article can be found, in the online version, at doi:10.1016/j.actbio.2020.04.030.

References

[1] B. Clarke, Normal bone anatomy and physiology, Clin. J. Am. Soc. Nephrol. 3 (Supplement 3) (2008) S131–S139.
[2] R. Weinkamer, P. Fratzl, Mechanical adaptation of biological materials - The examples of bone and wood, Mater. Sci. Eng. C. 31 (6) (2011) 1164–1173.
[3] C.H. Turner, Three rules for bone adaptation to mechanical stimuli, Bone 23 (5) (1998) 399–407.
[4] P. Augat, S. Schorlemmer, The role of cortical bone and its microstructure in bone strength, Age and Ageing 35 (S2) (2006) ii27–ii31.
[5] S. Weiner, T. Arad, I. Sabanay, W. Traub, Rotated plywood structure of primary lamellar bone in the rat: Orientations of the collagen fibril arrays, Bone 20 (6) (1997) 509–514.
[6] P. Varga, A. Pacureanu, M. Langer, H. Suhonen, B. Hesse, Q. Grimal, P. Cloetens, K. Raum, F. Peyrin, Investigation of the three-dimensional orientation of mineralized collagen fibrils in human lamellar bone using synchrotron X-ray phase nano-tomography, Acta Biomater 9 (9) (2013) 8118–8127.
[7] S. Weiner, W. Traub, H.D. Wagner, Lamellar bone: structure– function relations, J. Struct. Biol. 126 (3) (1999) 241–255.
[8] N. Reznikov, R. Shahar, S. Weiner, Three-dimensional structure of human lamellar bone: The presence of two different materials and new insights into the hierarchical organization, Bone 59 (2014) 93–104.
[9] P. Fratzl, H.S. Gupta, E.P. Paschalis, P. Roschger, Structure and mechanical quality of the collagen-mineral nano-composite in bone, J. Mater. Chem. 14 (14) (2004) 2115–2123.
[10] M.J. Buehler, Molecular nanomechanics of nascent bone: fibrillar toughening by mineralization, Nanotechnology 18 (29) (2007) 295102.
[11] J.Y. Rho, L. Kuhn-Spearing, P. Zioupos, Mechanical properties and the hierarchical structure of bone, Med. Eng. Phys. 20 (2) (1998) 92–102.
[12] U.G.K. Wegst, M.F. Ashby, The mechanical efficiency of natural materials, Philos. Mag. 84 (21) (2004) 2167–2186.
[13] H. Gao, Application of fracture mechanics concepts to hierarchical biomechanics of bone and bone-like materials, Int. J. Fract. 138 (1–4) (2006) 101–137.

[14] H. Gao, B. Ji, I.L. Jager, E. Arzt, P. Fratzl, Materials become insensitive to flaws at nanoscale: Lessons from nature, Proc. Natl. Acad. Sci. 100 (10) (2003) 5597–5600.
[15] B. Ji, H. Gao, Mechanical properties of nanostructure of biological materials, J. Mech. Phys. Solids. 52 (9) (2004) 1963–1990.
[16] B. Davies, A. King, P. Newman, A. Minett, C.R. Dunstan, H. Zreiqat, Hypothesis: Bones toughness arises from the suppression of elastic waves, Sci. Rep. 4 (7538) (2014).
[17] S. Viguet-Carrin, P. Garnero, P.D. Delmas, The role of collagen in bone strength, Osteoporos. Int. 17 (3) (2006) 319–336.
[18] H.S. Gupta, W. Wagermaier, G.A. Zickler, D.R. Ben Aroush, S.S. Funari, P. Roschger, H.D. Wagner, P. Fratzl, Nanoscale deformation mechanisms in bone, Nano Lett 5 (10) (2005) 2018–2111.
[19] G.E. Fantner, T. Hassenkam, J.H. Kindt, J.C. Weaver, H. Birkedal, L. Pechenik, J.A. Cutroni, G.A.G. Cidade, G.D. Stucky, D.E. Morse, P.K. Hansma, Sacrificial bonds and hidden length dissipate energy as mineralized fibrils separate during bone fracture, Nat. Mater. 4 (2005) 612–616.
[20] R.O. Ritchie, M.J. Buehler, P. Hansma, Plasticity and toughness in bone, Phys. Today 62 (6) (2009) 41–47.
[21] A.K. Nair, A. Gautieri, S.W. Chang, M.J. Buehler, Molecular mechanics of mineralized collagen fibrils in bone, Nat. Commun. 4 (2013).
[22] F. Hang, H.S. Gupta, A.H. Barber, Nanointerfacial strength between non-collagenous protein and collagen fibrils in antler bone, J. R. Soc. Interface. 11 (92) (2014).
[23] O.L. Katsamenis, H.M.H. Chong, O.G. Andriotis, P.J. Thurner, Load-bearing in cortical bone microstructure: Selective stiffening and heterogeneous strain distribution at the lamellar level, J. Mech. Behav. Biomed. Mater. 17 (2013) 152–165.
[24] M.E. Launey, M.J. Buehler, R.O. Ritchie, On the Mechanistic Origins of Toughness in Bone, Annu. Rev. Mater. Res. 40 (1) (2010) 25–53.
[25] F. Barthelat, Architectured materials in engineering and biology: Fabrication, structure, mechanics and performance, Int. Mater. Rev. 60 (8) (2015) 413–430.
[26] W. Wagermaier, K. Klaushofer, P. Fratzl, Fragility of Bone Material Controlled by Internal Interfaces, Calcif. Tissue Int. 97 (3) (2015) 201–212.
[27] U.G.K. Wegst, H. Bai, E. Saiz, A.P. Tomsia, R.O. Ritchie, Bioinspired structural materials, Nat. Mater. 14 (1) (2015) 23–36.
[28] M. Mirkhalaf, A.K. Dastjerdi, F. Barthelat, Overcoming the brittleness of glass through bio-inspiration and micro-architecture, Nat. Commun. 5 (2014).
[29] K. Engelke, B. van Rietbergen, P. Zysset, FEA to Measure Bone Strength: A Review, Clin. Rev. Bone Miner. Metab. 14 (1) (2016) 26–37.
[30] P. Varga, D.H. Pahr, S. Baumbach, P.K. Zysset, HR-pQCT based FE analysis of the most distal radius section provides an improved prediction of Colles' fracture load in vitro, Bone 47 (5) (2010) 982–988.
[31] M.D. Uchic, D.M. Dimiduk, J.N. Florando, W.D. Nix, Sample dimensions influence strength and crystal plasticity, Science 305 (5686) (2004) 986–989.
[32] J. Schwiedrzik, R. Raghavan, A. Bürki, V. Lenader, U. Wolfram, J. Michler, P. Zysset, In situ micropillar compression reveals superior strength and ductility but an absence of damage in lamellar bone, Nat. Mater. 13 (7) (2014) 740–747.
[33] K.W. Luczynski, A. Steiger-Thirsfeld, J. Bernardi, J. Eberhardsteiner, C. Hellmich, Extracellular bone matrix exhibits hardening elastoplasticity and more than double cortical strength: Evidence from homogeneous compression of non-tapered single micron-sized pillars welded to a rigid substrate, J. Mech. Behav. Biomed. Mater. 52 (2015) 51–62.
[34] O.A. Tertuliano, J.R. Greer, The nanocomposite nature of bone drives its strength and damage resistance, Nat. Mater. 15 (11) (2016) 1195–1202.
[35] J. Schwiedrzik, A. Taylor, D. Casari, U. Wolfram, P. Zysset, J. Michler, Nanoscale deformation mechanisms and yield properties of hydrated bone extracellular matrix, Acta Biomater 60 (2017) 302–314.
[36] A. Groetsch, A. Gourrier, J. Schwiedrzik, M. Sztucki, R.J. Beck, J.D. Shephard, J. Michler, P.K. Zysset, U. Wolfram, Compressive behaviour of uniaxially aligned individual mineralised collagen fibres at the micro- and nanoscale, Acta Biomater 89 (2019) 313–329.
[37] U. Wolfram, J.J. Schwiedrzik, M.J. Mirzaali, A. Bürki, P. Varga, C. Olivier, F. Peyrin, P.K. Zysset, Characterizing microcrack orientation distribution functions in osteonal bone samples, J. Microsc 264 (3) (2016) 268–281.
[38] D. Casari, L. Pethö, P. Schürch, X. Maeder, L. Philippe, J. Michler, P. Zysset, J. Schwiedrzik, A self-aligning microtensile setup: Application to single-crystal GaAs microscale tension–compression asymmetry, J. Mater. Res. 34 (14) (2019) 2517–2534.
[39] Y.H. An, R.A. Draughn, Mechanical testing of bone and the bone-implant interface, first ed., CRC Press, Boca Raton FL, 1999.
[40] R. Rezakhaniha, A. Agianniotis, J.T.C. Schrauwen, A. Griffa, D. Sage, C.V.C. Bouten, F.N. Van De Vosse, M. Unser, N. Stergiopulos, Experimental investigation of collagen waviness and orientation in the arterial adventitia using confocal laser scanning microscopy, Biomech. Model. Mechanobiol. 11 (3–4) (2012) 461–473.
[41] Z. Hashin, Failure criteria for unidirectional fiber composites, J. Appl. Mech. 47 (2) (1980) 329–334.
[42] J. Gu, P. Chen, Some modifications of Hashin's failure criteria for unidirectional composite materials, Compos. Struct. 182 (2017) 143–152.
[43] J.Y. Rho, M.E. Roy, T.Y. Tsui, G.M. Pharr, Elastic properties of microstructural components of human bone tissue as measured by nanoindentation, J. Biomed. Mater. Res. 45 (1) (1999) 48–54.
[44] J.Y. Rho, G.M. Pharr, Effects of drying on the mechanical properties of bovine femur measured by nanoindentation, J. Mater. Sci. Mater. Med. 10 (8) (1999) 485–488.
[45] X.J. Wang, X.B. Chen, P.D. Hodgson, C.E. Wen, Elastic modulus and hardness of cortical and trabecular bovine bone measured by nanoindentation, Trans. Nonferrous Met. Soc. China (English Edition) 16 (supplement 2) (2006) s744–s748.
[46] C.H. Turner, J. Rho, Y. Takano, T.Y. Tsui, G.M. Pharr, The elastic properties of trabecular and cortical bone tissues are similar: Results from two microscopic measurement techniques, J. Biomech. 32 (4) (1999) 437–441.
[47] Z. Fan, J.G. Swadener, J.Y. Rho, M.E. Roy, G.M. Pharr, Anisotropic properties of human tibial cortical bone as measured by nanoindentation, J. Orthop. Res. 20 (4) (2002) 806–810.
[48] J.Y. Rho, T.Y. Tsui, G.M. Pharr, Elastic properties of human cortical and trabecular lamellar bone measured by nanoindentation, Biomaterials 18 (20) (1997) 1325–1330.
[49] C. Edward Hoffler, X. Edward Guo, P.K. Zysset, S.A. Goldstein, An application of nanoindentation technique to measure bone tissue lamellae properties, J. Biomech. Eng. 127 (7) (2005) 1046–1053.
[50] W.C. Oliver, G.M. Pharr, An improved technique for determining hardness and elastic modulus using load and displacement sensing indentation experiments, J. Mater. Res. 7 (6) (1992) 1564–1583.
[51] G. Franzoso, P.K. Zysset, Elastic anisotropy of human cortical bone secondary osteons measured by nanoindentation, J. Biomech. Eng. 131 (2) (2009) 021001.
[52] A.G. Reisinger, D.H. Pahr, P.K. Zysset, Principal stiffness orientation and degree of anisotropy of human osteons based on nanoindentation in three distinct planes, J. Mech. Behav. Biomed. Mater. 4 (8) (2011) 2113–2127.
[53] A.G. Reisinger, D.H. Pahr, P.K. Zysset, Sensitivity analysis and parametric study of elastic properties of an unidirectional mineralized bone fibril-array using mean field methods, Biomech. Model. Mechanobiol. 9 (5) (2010) 499–510.
[54] E. Hamed, Y. Lee, I. Jasiuk, Multiscale modeling of elastic properties of cortical bone, Acta Mech 213 (1–2) (2010) 131–154.
[55] D.T. Reilly, A.H. Burstein, The elastic and ultimate properties of compact bone tissue, J. Biomech. 8 (6) (1975) 393–396.
[56] M.B. Schaffler, K. Choi, C. Milgrom, Aging and matrix microdamage accumulation in human compact bone, Bone 17 (6) (1995) 521–525.
[57] Y.N. Yeni, C.U. Brown, Z. Wang, T.L. Norman, The influence of bone morphology on fracture toughness of the human femur and tibia, Bone 21 (5) (1997) 453–459.
[58] R.K. Nalla, J.J. Kruzic, J.H. Kinney, M. Balooch, J.W. Ager, R.O. Ritchie, Role of microstructure in the aging-related deterioration of the toughness of human cortical bone, Mater. Sci. Eng. C. 26 (8) (2006) 1251–1260.
[59] J. Jowsey, Studies of Haversian systems in man and some animals, J. Anat. 100 (4) (1966) 857–864.
[60] M.J. Mirzaali, J.J. Schwiedrzik, S. Thaiwichai, J.P. Best, J. Michler, P.K. Zysset, U. Wolfram, Mechanical properties of cortical bone and their relationships with age, gender, composition and microindentation properties in the elderly, Bone 93 (2016) 196–211.
[61] M. Tzaphlidou, The role of collagen in bone structure: An image processing approach, Micron 36 (7–8) (2005) 593–601.
[62] F. Repp, P. Kollmannsberger, A. Roschger, A. Berzlanovich, G.M. Gruber, P. Roschger, W. Wagermaier, R. Weinkamer, Coalignment of osteocyte canaliculi and collagen fibers in human osteonal bone, J. Struct. Biol. 199 (3) (2017) 177–186.
[63] N. Reznikov, R. Almany Magal, R. Shahar, S. Weiner, Three-dimensional imaging of collagen fibril organization in rat circumferential lamellar bone using a dual beam electron microscope reveals ordered and disordered sub-lamellar structures, Bone 52 (2) (2013) 676–683.
[64] E. Giner, C. Arango, A. Vercher, F. Javier Fuenmayor, Numerical modelling of the mechanical behaviour of an osteon with microcracks, J. Mech. Behav. Biomed. Mater. 37 (2014) 109–124.
[65] P. Fratzl, Bone fracture: When the cracks begin to show, Nat. Mater. 7 (8) (2008) 610–612.
[66] K.J. Koester, J.W. Ager, R.O. Ritchie, The true toughness of human cortical bone measured with realistically short cracks, Nat. Mater. 7 (8) (2008) 672–677.
[67] D.B. Burr, M.B. Schaffler, R.G. Frederickson, Composition of the cement line and its possible mechanical role as a local interface in human compact bone, J. Biomech. 21 (11) (1988) 939–941.
[68] S. Mohsin, F.J. O'Brien, T.C. Lee, Osteonal crack barriers in ovine compact bone, J. Anat. 208 (1) (2006) 81–89.
[69] T.L. Anderson, Fracture Mechanics: Fundamentals and Applications, fourth ed., CRC Press, Boca Raton FL, 2017.
[70] H. Tada, P.C. Paris, G.R. Irwin, The Stress Analysis of Cracks Handbook, second ed., ASME Press, St. Louis MO, 1985.
[71] O.A. Tertuliano, Small-scale Deformation and Fracture of Hard Biomaterials, California Institute of Technology, Pasadena CA, 2019.
[72] W.J. Landis, K.J. Hodgens, J. Arena, M.J. Song, B.F. McEwen, Structural relations between collagen and mineral in bone as determined by high voltage electron microscopic tomography, Microsc. Res. Tech. 33 (2) (1996) 192–202.
[73] J.R. Taylor, An introduction to error analysis: The Study of Uncertainties in Physical Measurements, University Science Books, Mill Valley CA, 1982.
[74] H.D. Wagner, S. Weiner, On the relationship between the microstructure of bone and its mechanical stiffness, J. Biomech. 25 (11) (1992) 1311–1320.

Please cite this article as: D. Casari, J. Michler and P. Zysset et al., Microtensile properties and failure mechanisms of cortical bone at the lamellar level, Acta Biomaterialia, https://doi.org/10.1016/j.actbio.2020.04.030

[75] R.M.V. Pidaparti, A. Chandran, Y. Takano, C.H. Turner, Bone mineral lies mainly outside collagen fibrils: Predictions of a composite model for osteonal bone, J. Biomech. 29 (7) (1996) 909–916.
[76] W. Wagermaier, H.S. Gupta, A. Gourrier, M. Burghammer, P. Roschger, P. Fratzl, Spiral twisting of fiber orientation inside bone lamellae, Biointerphases 1 (1) (2006) 1–5.
[77] E.M. Spiesz, W. Kaminsky, P.K. Zysset, A quantitative collagen fibers orientation assessment using birefringence measurements: Calibration and application to human osteons, J. Struct. Biol. (2011).
[78] C.H. Turner, A. Chandran, R.M.V. Pidaparti, The anisotropy of osteonal bone and its ultrastructural implications, Bone 17 (1) (1995) 85–89.
[79] H. Peterlik, P. Roschger, K. Klaushofer, P. Fratzl, From brittle to ductile fracture of bone, Nat. Mater. 5 (1) (2006) 52–55.
[80] H.S. Gupta, U. Stachewicz, W. Wagermaier, P. Roschger, H.D. Wagner, P. Fratzl, Mechanical modulation at the lamellar level in osteonal bone, J. Mater. Res. 21 (8) (2006) 1913–1921.
[81] J. Schwiedrzik, R. Raghavan, M. Rüggeberg, S. Hansen, J. Wehrs, R.B. Adusumalli, T. Zimmermann, J. Michler, Identification of polymer matrix yield stress in the wood cell wall based on micropillar compression and micromechanical modelling, Philos. Mag. 96 (32–34) (2016) 3461–3478.
[82] A. Speed, A. Groetsch, J.J. Schwiedrzik, U. Wolfram, Extrafibrillar matrix yield stress and failure envelopes for mineralised collagen fibril arrays, J. Mech. Behav. Biomed. Mater. (2019) 103563.
[83] M. Ferretti, M.A. Muglia, F. Remaggi, V. Canè, C. Palumbo, Histomorphometric study on the osteocyte lacuno-canalicular network in animals of different species. II. Parallel-fibered and lamellar bones, Ital. J. Anat. Embryol. 104 (3) (1999) 121–131.
[84] L. Cardoso, S.P. Fritton, G. Gailani, M. Benalla, S.C. Cowin, Advances in assessment of bone porosity, permeability and interstitial fluid flow, J. Biomech. 46 (2) (2013) 253–265.
[85] A. Roschger, S. Gamsjaeger, B. Hofstetter, A. Masic, S. Blouin, P. Messmer, A. Berzlanovich, E.P. Paschalis, P. Roschger, K. Klaushofer, P. Fratzl, Relationship between the v2PO4/amide III ratio assessed by Raman spectroscopy and the calcium content measured by quantitative backscattered electron microscopy in healthy human osteonal bone, J. Biomed. Opt. 19 (6) (2014) 065002.
[86] M. Kazanci, P. Roschger, E.P. Paschalis, K. Klaushofer, P. Fratzl, Bone osteonal tissues by Raman spectral mapping: Orientation-composition, J. Struct. Biol. 156 (3) (2006) 489–496.
[87] S. Gamsjaeger, B. Hofstetter, N. Fratzl-Zelman, P. Roschger, A. Roschger, P. Fratzl, W. Brozek, A. Masic, B.M. Misof, F.H. Glorieux, K. Klaushofer, F. Rauch, E.P. Paschalis, Pediatric reference Raman data for material characteristics of iliac trabecular bone, Bone 69 (2014) 89–97.
[88] D.P. Clausing, Crack stability in linear elastic fracture mechanics, Int. J. Fract. Mech. 5 (3) (1969) 211–227.
[89] J. Seto, H.S. Gupta, P. Zaslansky, H.D. Wagner, P. Fratzl, Tough lessons from bone: Extreme mechanical anisotropy at the mesoscale, Adv. Funct. Mater. 18 (13) (2008) 1905–1911.
[90] P.K. Zysset, X. Edward Guo, C. Edward Hoffler, K.E. Moore, S.A. Goldstein, Elastic modulus and hardness of cortical and trabecular bone lamellae measured by nanoindentation in the human femur, J. Biomech 32 (10) (1999) 1005–1012.
[91] O.G. Andriotis, S. Desissaire, P.J. Thurner, Collagen Fibrils: Nature's Highly Tunable Nonlinear Springs, ACS Nano 12 (4) (2018) 3671–3680.
[92] Z.L. Shen, H. Kahn, R. Ballarini, S.J. Eppell, Viscoelastic properties of isolated collagen fibrils, Biophys. J. 100 (12) (2011) 3008–3015.
[93] S. Pathak, J. Gregory Swadener, S.R. Kalidindi, H.W. Courtland, K.J. Jepsen, H.M. Goldman, Measuring the dynamic mechanical response of hydrated mouse bone by nanoindentation, J. Mech. Behav. Biomed. Mater. 4 (1) (2011) 34–43.
[94] M. Maghsoudi-Ganjeh, L. Lin, X. Wang, X. Zeng, Computational investigation of ultrastructural behavior of bone using a cohesive finite element approach, Biomech. Model. Mechanobiol. 18 (2) (2019) 463–478.
[95] A. Fritsch, C. Hellmich, L. Dormieux, Ductile sliding between mineral crystals followed by rupture of collagen crosslinks: Experimentally supported micromechanical explanation of bone strength, J. Theor. Biol. 260 (2) (2009) 230–252.
[96] H.S. Gupta, W. Wagermaier, G.A. Zickler, J. Hartmann, S.S. Funari, P. Roschger, D.H. Wagner, P. Fratzl, Fibrillar level fracture in bone beyond the yield point, Int. J. Fract. 139 (3–4) (2006) 425–436.
[97] J. Samuel, J.S. Park, J. Almer, X. Wang, Effect of water on nanomechanics of bone is different between tension and compression, J. Mech. Behav. Biomed. Mater. 57 (2016) 128–138.
[98] G. Lewis, J.S. Nyman, The use of nanoindentation for characterizing the properties of mineralized hard tissues: State-of-the art review, J. Biomed. Mater. Res. - Part B Appl. Biomater. 87 (1) (2008) 286–301.
[99] L. Feng, M. Chittenden, J. Schirer, M. Dickinson, I. Jasiuk, Mechanical properties of porcine femoral cortical bone measured by nanoindentation, J. Biomech 45 (10) (2012) 1775–1782.
[100] H.S. Gupta, J. Seto, W. Wagermaier, P. Zaslansky, P. Boesecke, P. Fratzl, Cooperative deformation of mineral and collagen in bone at the nanoscale, Proc. Natl. Acad. Sci. 103 (47) (2006) 17741–17746.
[101] R.K. Nalla, J.H. Kinney, R.O. Ritchie, Mechanistic fracture criteria for the failure of human cortical bone, Nat. Mater. 2 (3) (2003) 164–168.

Please cite this article as: D. Casari, J. Michler and P. Zysset et al., Microtensile properties and failure mechanisms of cortical bone at the lamellar level, Acta Biomaterialia, https://doi.org/10.1016/j.actbio.2020.04.030